FULL PAPER

Graphene Reinforced Carbon Nanotube Networks for Wearable Strain Sensors

Jidong Shi, Xinming Li, Huanyu Cheng, Zhuangjian Liu, Lingyu Zhao, Tingting Yang, Zhaohe Dai, Zengguang Cheng, Enzheng Shi, Long Yang, Zhong Zhang, Anyuan Cao, Hongwei Zhu,* and Ying Fang**

Transparent, stretchable films of carbon nanotubes (CNTs) have attracted significant attention for applications in flexible electronics, while the lack of structural strength in CNT networks leads to deformation and failure under high mechanical load. In this work, enhancement of the strength and load transfer capabilities of CNT networks by chemical vapor deposition of graphene in the nanotube voids is proposed. The graphene hybridization significantly strengthens the CNT networks, especially at nanotube joints, and enhances their resistance to buckling and bundling under large cyclic strain up to 20%. The hybridized films show linear and reproducible responses to tensile strains, which have been applied in strain sensors to detect human motions with fast response, high sensitivity, and durability.

1. Introduction

Flexible electronics have been studied extensively for many applications in recent years, including malleable displays, wearable devices, and implantable biosensors.[1–8] Networks of overlapping 1D nanostructures have been favorably used as functional materials in flexible electronics owing not only to their superior stretchability but also to their outstanding conductivity and transparency.[9,10] Thin films of copper nanowires,[11] silver nanowires,[12] and carbon nanotubes (CNTs)[13,14] are all commonly used to construct flexible devices. Among these nanostructures, CNT networks are of particular interest due to their low-cost and scalable synthesis, as well as good chemical stability.[15–18] Carbon nanotubes are joined by the van der Waals forces and form entangled networks. Due to the weak interactions at the nanotube joints, the networks can respond to tensile loads through interfacial sliding between neighboring nanotubes, which reduces the number density of nanotube joints and consequently decreases the electrical conductivity of the networks.[19] This property of the CNT films can be employed to measure strains and monitor motions.[13,14] However, due to the flexibility of 1D nanostructures, CNTs bend and buckle (instead of slide back) upon the release of loads, which results in wavy structures in the network.[14,20] The generation of nanotube buckles prevents the restoration of conductive paths in the network after releasing the strain, leading to permanent loss in network conductivity.[21,22] In addition, upon cyclic loads, the wavy CNTs are first straightened under tensile strain, causing no/little change in conductivity. These microstructural deformation processes in CNT networks seriously compromise their reliability and accuracy as strain sensors. Therefore, the major challenge for CNT networks, as well as other 1D networks, is to tackle the weak nanotube joints to resist buckling deformation. It has been shown that the mechanical strength of 3D, porous CNT foams can be greatly improved by the addition of graphene oxide fillers through hydrothermal[23] or dip-coating processes.[24,25] However, these methods always result in inhomogeneous distribution of fillers in the matrix, which could compromise the

J. D. Shi, Dr. X. M. Li, L. Y. Zhao, Z. H. Dai, Dr. Z. G. Cheng, L. Yang, Prof. Z. Zhang, Prof. Y. Fang
National Center for Nanoscience and Technology
Beijing 100190, P. R. China
E-mail: fangy@nanoctr.cn; lixm2@nanoctr.cn
Prof. H. Cheng
Department of Engineering Science and Mechanics
Materials Research Institute
The Pennsylvania State University
University Park, PA 16802, USA
Dr. Z. J. Liu
Institute of High Performance Computing
1 Fusionopolis Way, #16-16 Connexis,
A*Star, Singapore 138632, Singapore

DOI: 10.1002/adfm.201504804

T. T. Yang, Prof. H. W. Zhu
State Key Laboratory of New Ceramics and Fine Processing
School of Materials Science and Engineering
Tsinghua University
Beijing 100084, P. R. China
E-mail: hongweizhu@tsinghua.edu.cn
Dr. E. Z. Shi, Prof. A. Y. Cao
Department of Materials Science and Engineering
College of Engineering
Peking University
Beijing 100871, P. R. China
Prof. Y. Fang
CAS Center for Excellence in Brain Science and Intelligence Technology
320 Yue Yang Road, Shanghai 200031, P. R. China

mechanical performance of the foams.[26] In addition, solution-based processes are known to cause the reduction in electrical conductivity of CNT networks.[23]

In this work, we present a novel strain sensor based on a chemically hybridized film of CNT and graphene. Chemical vapor deposition (CVD) growth of graphene on copper was carried out by using ultrathin CNT films as templates, in which graphene homogeneously fills the nanotube voids and forms a seamless hybrid, named CNT embroidered graphene (CeG). We systematically investigated the microstructural evolution of the CeG films under cyclic strains. The graphene hybridization greatly improves the strength and load transfer at the nanotube joints, while maintaining the high transparency and conductivity of the CNT networks. Significantly, the buckling behavior of nanotubes after cyclic strains has been completely prevented in CeG films, even at a strain of 20%. As a result, the CeG films exhibit linear and reliable conductivity responses to cyclic strains. The CeG films have been applied as strain sensors to detect human finger motions with fast response and high accuracy, demonstrating their potential for applications in wearable devices.

2. Results and Discussions

2.1. Preparation and Characterization

Thin CNT films were prepared by a floating catalyst CVD method, and the thickness and conductivity of the films were controlled by adjusting the growth time. Due to the porous structure, CNT films offer high optical transparency. For this work, we chose ultrathin CNT films with a high transmittance of 90.2% at 550 nm (Figure S1, Supporting Information) and a sheet resistance of ≈4 kΩ sq^{-1}. CeG films were synthesized through catalytic growth of graphene by using ultrathin CNT films as porous templates, resulting in seamless CNT–graphene hybrids (**Figure 1**a). After graphene hybridization, the transmittance of the CeG changes slightly to 87.1% at 550 nm (Figure S1, Supporting Information), indicating its potential applications in transparent devices. To fabricate flexible devices, liquid polydimethylsiloxane (PDMS) was poured onto the as-synthesized CeG films and cured overnight at room temperature. The use of liquid PDMS helps to increase the adhesion between CeG films and PDMS. After copper etching, metal wires were connected to CeG films, as shown in Figure S2 (Supporting Information) and illustrated in detail in the Experimental Section. We note that the CeG films show no obvious change in sheet resistance compared to pristine CNT films. This result confirms that the CNT networks dominate the conductance of the hybrids. More importantly, in contrast to previous solution-based approaches, our method ensures that the conductive paths in the CNT networks remain intact after graphene hybridization.

Figure 1b presents the scanning electron microscope (SEM) images of an ultrathin CNT film before and after graphene hybridization. The pristine CNT film consists of randomly interconnected CNTs, with tube length from several micrometers to tens of micrometers (Figure 1b (i)). Whereas in the CeG film, CVD grown graphene, predominantly single-layer, homogeneously fills in the nanotube voids, forming a continuous CNT–graphene hybrid (Figure 1b (ii)). The in situ synthesis of the hybrid ensures a strong interaction between CNT and graphene. These structural features closely resemble those of leaves and insects wings consisting of supporting veins and flexible membranes, with both factors acting together to achieve desirable mechanical properties (Figure 1b (iii)).

2.2. Resistance to Buckling of CeG

2.2.1. Microstructural Analysis upon Cyclic Loads

To investigate the role of graphene hybridization, we characterized the microstructural evolution of both CNT and CeG films under cyclic tensile strains. As shown in **Figure 2**a, flat CNT films buckled and developed into periodic, wavy structures after repeatedly stretching and releasing with a strain of 10%. When the tensile strain was increased to 20%, more buckles appeared in CNT films, with increased height and decreased wavelength, respectively (Figure S3, Supporting Information). These deformation processes of the CNT network are irreversible and result

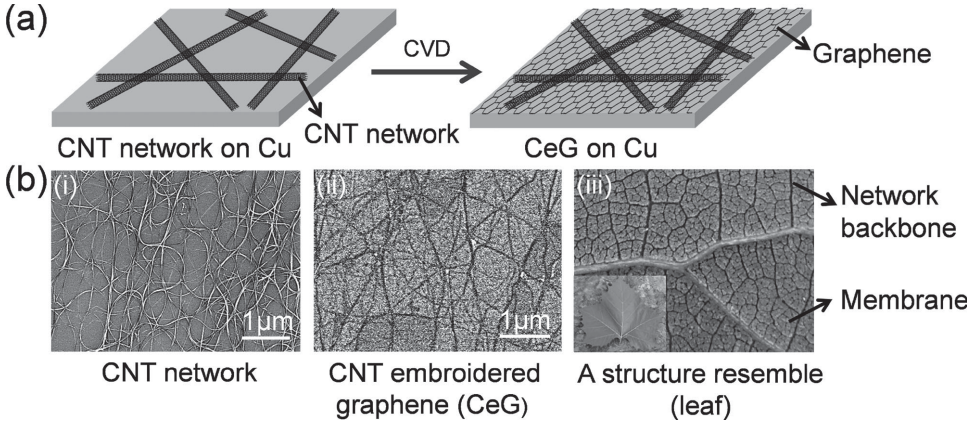

Figure 1. a) Schematic illustration of the synthesis of a CNT embroidered graphene (CeG) film by using ultrathin CNT network as template. b) SEM images of ultrathin CNT network (i) and derived CeG (ii), along with the optical images of a phoenix tree leaf (iii).

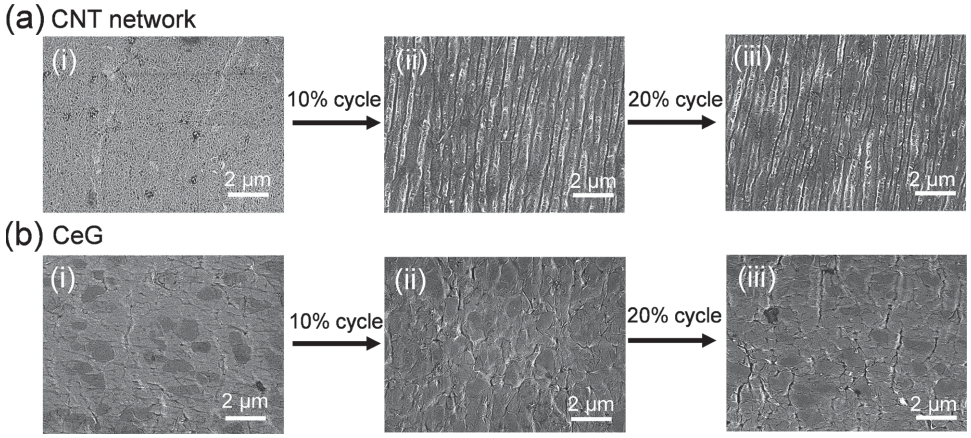

Figure 2. Morphological analysis of both CNT film and CeG film under cyclic tensile strain. a) SEM images of a CNT film before stretch (i), after cyclic stretch and release at a strain of 10% (ii), after cyclic stretch and release at a strain of 20% (iii). b) SEM images of a CeG film before stretch (i), after cyclic stretch and release at a strain of 10% (ii), after cyclic stretch and release at a strain of 20% (iii).

in considerable energy dissipation. On the other hand, the buckling of CNTs has been effectively prevented by graphene hybridization. The CeG film was flat and showed no buckling after cyclic strain up to 20%, as shown in Figure 2b. Instead, microscale cracks were formed in the CeG film. Interestingly, the microscale cracks usually follow the junctions between CNT and graphene, and are not restricted to the transverse direction.

2.2.2. Theoretical Analysis of the Role of Hybridized Graphene

To validate the buckling-resistant ability of graphene hybridization, we carried out 3D finite element analysis to reveal the mechanism of hybridized graphene enhanced mechanical properties in the CNT networks. In a representative model, a CNT network consisting of three nanotubes in an equilateral triangular pattern is attached onto a PDMS substrate (**Figure 3**a (i) and (ii)). Under a uniaxial stretching in the *x* direction, the two nanotubes at the right and left sides of the triangle bend outward (Figure 3a (iii)), as a result of the vertical compression induced by the Poisson effect. The elongation of the third nanotube at the base side is small due to the high Young's modulus of CNTs. Compared with the pristine CNT network, a CNT–graphene hybrid is mechanically stronger. Under the same tensile strain, the CNTs at the right and left sides of the triangular hybrid show much smaller deformation than the pristine CNT network (Figure 3a (iv)), demonstrating an enhanced strength. In addition, the maximum principal strain at the three nanotube junctions of the CNT–graphene hybrid is also much smaller than that of the pristine CNT network (Figure 3a (iii, iv) and Figure S4, Supporting Information), indicating the effective load transfer within the CNT–graphene hybrid. These

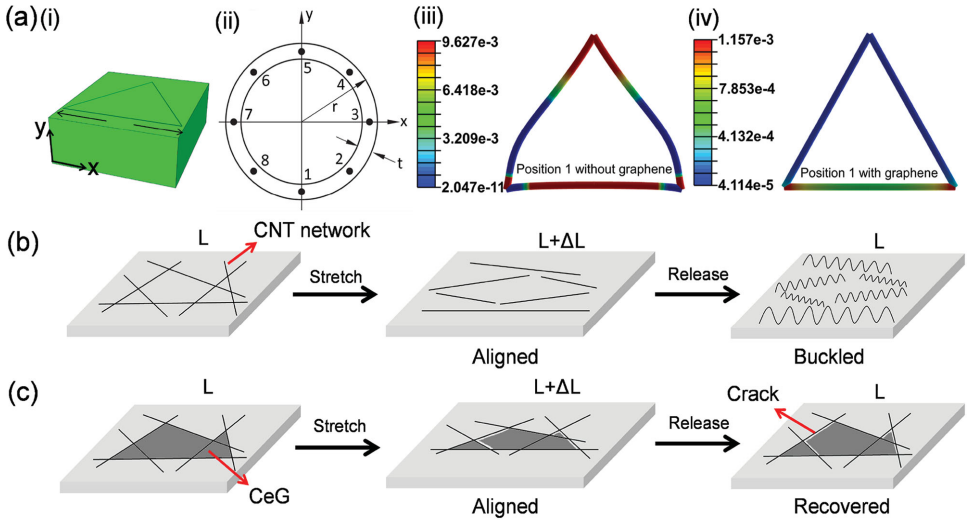

Figure 3. Mechanism for graphene-enhanced mechanical properties in CNT network. a) Finite element method (FEM) analysis of graphene hybridization. (i) Schematic of an equilateral triangular CNT network unit attached on a PDMS substrate, and the direction of the tensile strain is marked by the arrows. (ii) Cross sectional schematic of a carbon nanotube. Eight positions are chosen for the analysis of strain distribution, with the adjacent positions staggered by 45°. (iii, iv) The spatial distribution of the maximum principal strain at position 1 for the CNT network (iii) and CNT–graphene hybrid (iv), respectively, under a strain of 20%. b,c) Schematic illustration of the microstructural evolution of CNT network b) and CeG c) under stretch and release.

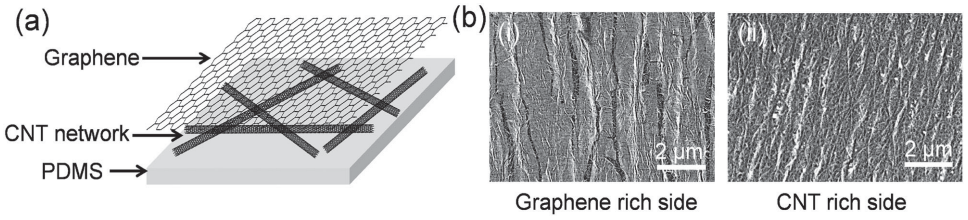

Figure 4. Microstructural analysis of layered CNT–graphene hybrid under cyclic strain. a) Schematic of a layered CNT–graphene hybrid. b) SEM images at the graphene-rich side (i) and the CNT-rich side (ii) of a layered CNT–graphene hybrid after cyclic stretch and release at a strain of 20%.

results indicate that the hybridized graphene can both increase the strength and reinforce the intertube junctions of the CNT network, which effectively prevents the buckling deformation of the CNT networks upon cyclic strain (Figure 3b,c).

2.2.3. Strong Interaction between CNT and Graphene in CeG

For comparison, we also prepared a layered CNT–graphene hybrid by van der Waals stacking of a CNT film with a graphene film,[27] as shown in **Figure 4**a and Figure S5 (Supporting Information). After cyclic strain, long transverse cracks are formed in the top graphene film of the layered hybrid (Figure 4b (i)), indicating that the load is homogenously transferred to the whole graphene film. These macroscopic, propagating cracks are distinctly different from the microscopic, localized cracks in the CeG films. In addition, the buckling of the CNT network can be clearly observed in the layered hybrid after cyclic loads (Figure 4b (ii)). These results confirm that the mechanical performance of CNT–graphene hybrid depends critically on the interaction between CNT and graphene. During the synthesis of the CeG films, graphene and CNTs are bonded to form a seamless hybrid, ensuring a strong interaction and effective load transfer within the CNT–graphene hybrid (Figure S6a, Supporting Information). On the other hand, the van der Waals interaction between graphene and CNTs in the layered hybrid is weak, and the load transfer between them is not as efficient to resist CNT buckling (Figure S6b, Supporting Information).

2.3. CeG as Strain Sensors

2.3.1. Electrical Analysis upon Cyclic Stretch and Release

Practical strain measurements require stretchable sensors with accurate and reproducible response under large strains. **Figure 5** characterizes the resistance response of both CNT films and CeG films under cyclic tensile strains. Both films were prestretched and released at a strain of 10%. The resistance of the films was then monitored in real-time when continuous triangular waves were applied with increasing peak strain from 1% to 10%. Five triangle wave tests were conducted for each peak strain level. Consistent with former studies,[14,20,22] the CNT film shows weak and nonmonotonic resistance response to tensile strains below 6% (Figure 5a). Counterintuitively, a small resistance peak appears for the CNT film at the release of the small strain, as shown in Figure 5b. This abnormality can be explained by the previously formed wavy structures of the CNT film. Under tensile loads, the buckled CNTs are first straightened and flattened, which slightly increases the contact area between nanotubes.[22] As a result, the resistance is decreased first under small strain loading. As the strain is further increased above 6%, the resistance of the CNT film starts to increase due to the reduction of nanotube joints, resulting in a second resistance peak at the maximum tensile strain (Figure 5c). Thus the buckling deformation processes of the CNT films lead to nonmonotonic response to strains, which seriously limits their applications as accurate strain sensors. On the other hand, the response of the CeG film is approximately linear (Figure 5c). The enhanced performance of the CeG film is consistent with the increased structural stability of the CNT network by graphene hybridization. The gauge factor of the CeG strain sensor is 0.36, which is comparable to PDMS supported CNT strain sensors at the first stretch.[14,20,22,28] Compared with other graphene and CNT strain sensors,[29–31] our CeG based strain sensors offer the advantages of high linearity and reproducibility under cyclic strains.

2.3.2. Application of CeG as Strain Sensors

The sensitive and linear response of the CeG films to strains, combined with their high transparency and flexibility, makes them particularly attractive for the development of strain sensors. As an example, transparent strain sensors based on CNT and CeG films have been fabricated to detect the bending movements of fingers (**Figure 6**a). As shown in Figure 6b, the CeG sensor is stretched during the bending of the index finger, which induces a fast and sensitive resistance response in the CeG film. As the finger is unfolded, the resistance of the CeG quickly returns to the base level. Whereas, for the CNT sensor, the bending-unbending motion of the finger results in a weak, negative resistance response due to the straightening processes of the CNT buckles. In addition, a three-channel CeG sensor has been further demonstrated to simultaneously measure the strains at different positions along the index finger during periodical bending and unbending (Figure S8, Supporting Information). These results demonstrate the unique potential of CeG films as transparent and reliable strain sensors.

3. Conclusion

In conclusion, we reported a flexible and transparent strain sensor based on chemically hybridized films of CNT and graphene, and demonstrated its practical application as wearable

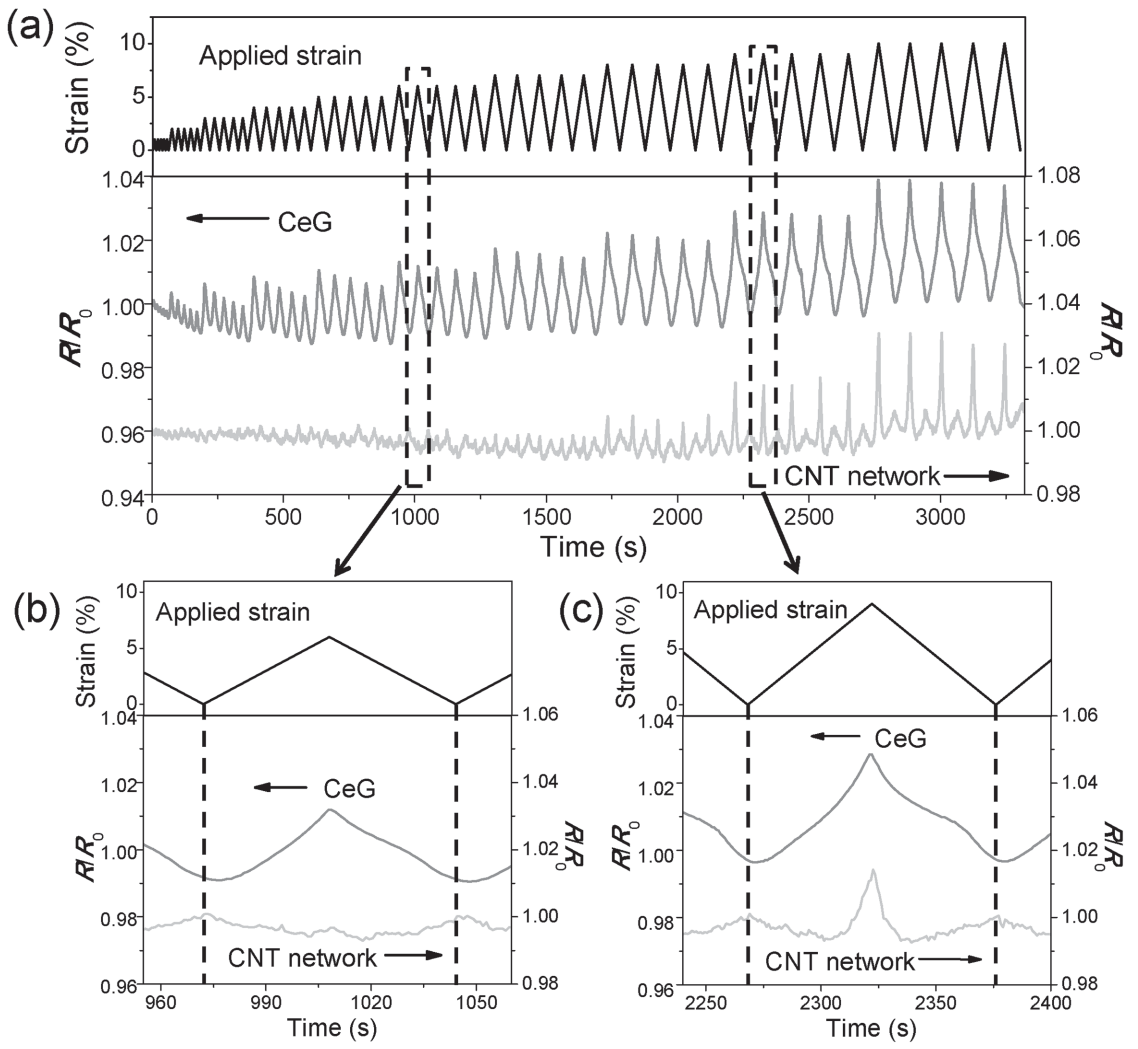

Figure 5. Resistance response of CNT film and CeG film during cyclic tensile stretch. a) Resistance recording of a CNT film and a CeG film under continuous triangular waves with increasing peak strain from 1% to 10%. Five triangle wave tests were conducted for each peak strain level. b) The magnified view of a triangle wave test with the peak strain of 6%. c) The magnified view of a triangle wave test with the peak strain of 9%.

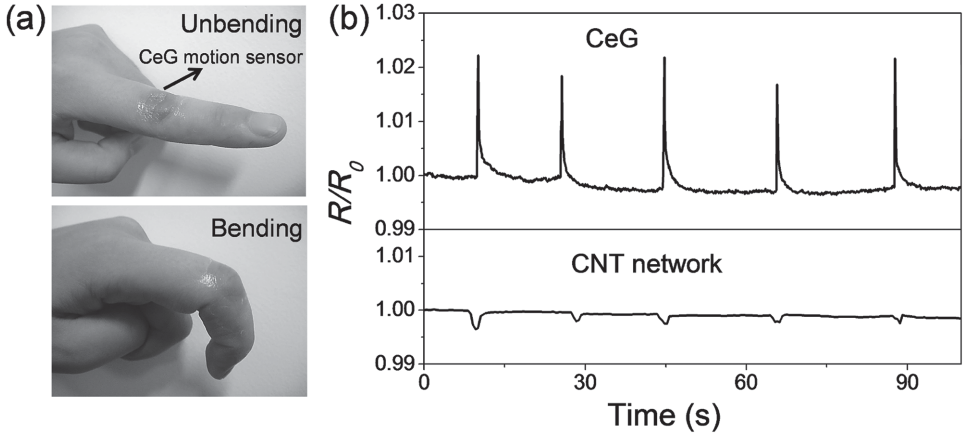

Figure 6. Demonstration of the motion sensing application of CeG. a) The photos of the unbending/bending state of a finger, with the CeG/ultrathin PDMS adhered on the finger joint. b) The resistance recording during five bending–releasing processes using CNT network and CeG based flexible device, respectively.

strain sensors. The graphene hybridization effectively resists the buckling deformation of CNTs under cyclic strain due to the strong interaction and effective load transfer within the hybridized films. As a result, the hybridized films exhibit linear and reliable resistance response to strain, which has been applied as wearable strain sensors to detect human motions. Our study highlights the strength and potential of smart material hybridization and may provide a new material platform for wearable and implantable electronics.

4. Experimental Section

Synthesis of CNT Films: CNT films were synthesized by floating catalyst CVD.[32] A quartz tube was heated to 1060 °C under 20 sccm Ar gas flow, then a xylene solution carrying ferrocene (0.045 g mL^{-1}) and sulfur (0.001 g mL^{-1}) was injected into the quartz tube in the upstream at 5 mL min^{-1}, with 1275 sccm Ar and 225 sccm H_2 flow. The reaction time could be adjusted from 5 to 60 min to control the thickness of CNT film. The as-prepared CNT films were collected on a nickel foil placed in the downstream of the gas flow. After synthesis, the CNT films were transferred onto water surface.

Preparation of CNT Embroidered Graphene (CeG): A CNT film was transferred to a Cu foil (Alfa, 99.99%). The CNT covered Cu foil was loaded into the quartz tube. Then the quartz tube was heated to 1050 °C under 8 sccm H_2 flow. After 30 min annealing, 10 sccm CH_4 was introduced into the quartz tube for graphene growth. After a growth time of 30 min, the quartz tube was cooled down to room temperature.[33]

Preparation of CeG Flexible Devices: The base and curing Agent of PDMS (Dow Corning Sylgard 184) were mixed in 10:1 mass ratio, and the wet PDMS was poured onto a CeG covered Cu foil after degassing. Then PDMS was cured at room temperature overnight, followed by the etching of Cu with 0.3 mol L^{-1} $FeCl_3$ aqueous solution. The membranes were rinsed twice with distilled water to remove $FeCl_3$ residual and then dried in air. Silver wires were attached to two ends of the CeG film for electrical measurements.

Mechanical and Electrical Characterizations: Tensile strains were applied by a dynamic mechanical analyzer manufactured by TA Instruments Company. Resistance recording was conducted in situ by a Keithley 4200-SCS Semiconductor parameter analyzer.

Finite Element Analysis Simulation: In a representative model, a CNT network consisting of three CNTs in an equilateral triangular pattern is bonded on the PDMS substrate. For CNT, the elastic modulus is set at 1TPa, the Poisson's ratio is 0.19; for graphene, the elastic modulus is 250 GPa, the Poisson's ratio is 0.16; for PDMS, the elastic modulus is 1.8 MPa, the Poisson's ratio is 0.49. All dimensions in the model were amplified by 1000 times into continuum region. The tensile strain is 20% in the horizontal direction. The maximum principal strain at eight positions along the nanotube cross section was investigated. Positions 6, 7, and 8 were omitted for discussion because they are symmetric to positions 2, 3, and 4, respectively. The maximum principal strain distribution of position 1 is presented in Figure 3a (iii, iv) and the maximum principal strain distributions of positions 2–5 are presented in Figure S4.

Supporting Information

Supporting Information is available from the Wiley Online Library or from the author.

Acknowledgements

J.D.S. and X.M.L. contributed equally to this work. This work was supported by the National Natural Science Foundation of China (51402060, 21322302) and the Strategic Priority Research Program of the Chinese Academy of Sciences (XDB02050008). H.C. acknowledges the start-up fund provided by the Department of Engineering Science and Mechanics, College of Engineering, and Materials Research Institute at The Pennsylvania State University. The authors thank Dr. Hongbian Li and Mingde Du from National Center for Nanoscience and Technology and Shiting Wu and Wenjing Xu from Peking University for the discussions.

Note: Figures were corrected on April 5, 2016.

Received: November 9, 2015
Revised: December 16, 2015
Published online: February 5, 2016

[1] S. R. Forrest, *Nature* **2004**, *428*, 911.
[2] M. L. Hammock, A. Chortos, B. C. K. Tee, J. B. H. Tok, Z. Bao, *Adv. Mater.* **2013**, *25*, 5997.
[3] X. Li, R. J. Zhang, W. J. Yu, K. L. Wang, J. Q. Wei, D. H. Wu, A. Y. Cao, Z. H. Li, Y. Cheng, Q. S. Zheng, R. S. Ruoff, H. W. Zhu, *Sci. Rep.* **2012**, *2*, 870.
[4] S. W. Hwang, C. H. Lee, H. Cheng, J.-W. Jeong, S.-K. Kang, J.-H. Kim, J. Shin, J. Yang, Z. Liu, G. A. Ameer, Y. Huang, J. A. Rogers, *Nano Lett.* **2015**, *15*, 2801.
[5] X. Zang, M. Zhu, X. Li, X. Li, Z. Zhen, J. Lao, K. Wang, F. Kang, B. Wei, H. Zhu, *Nano Energy* **2015**, *15*, 83.
[6] A. Chortos, G. I. Koleilat, R. Pfattner, D. Kong, P. Lin, R. Nur, T. Lei, H. Wang, N. Liu, Y.-C. Lai, M.-G. Kim, J. W. Chung, S. Lee, Z. Bao, *Adv. Mater.* **2015**, DOI: 10.1002/adma.201501828.
[7] T. Yang, W. Wang, H. Zhang, X. Li, J. Shi, Y. He, Q.-S. Zheng, Z. Li, H. Zhu, *ACS Nano* **2015**, *9*, 10867.
[8] X. Li, T. Yang, Y. Yang, J. Zhu, L. Li, F. E. Alam, X. Li, K. Wang, H. Cheng, C.-T. Lin, Y. Fang, H. Zhu, *Adv. Funct. Mater.* **2016**, *26*, 1322.
[9] L. Hu, H. S. Kim, J.-Y. Lee, P. Peumans, Y. Cui, *ACS Nano* **2010**, *4*, 2955.
[10] D. S. Leem, A. Edwards, M. Faist, J. Nelson, D. D. Bradley, J. C. de Mello, *Adv. Mater.* **2011**, *23*, 4371.
[11] Y. Cheng, S. Wang, R. Wang, J. Sun, L. Gao, *J. Mater. Chem. C* **2014**, *2*, 5309.
[12] D. Langley, G. Giusti, C. Mayousse, C. Celle, D. Bellet, J.-P. Simonato, *Nanotechnology* **2013**, *24*, 452001.
[13] T. Yamada, Y. Hayamizu, Y. Yamamoto, Y. Yomogida, A. Izadi-Najafabadi, D. N. Futaba, K. Hata, *Nat. Nanotechnol.* **2011**, *6*, 296.
[14] D. J. Lipomi, M. Vosgueritchian, B. C. Tee, S. L. Hellstrom, J. A. Lee, C. H. Fox, Z. Bao, *Nat. Nanotechnol.* **2011**, *6*, 788.
[15] T. Guo, P. Nikolaev, A. Thess, D. Colbert, R. Smalley, *Chem. Phys. Lett.* **1995**, *243*, 49.
[16] T. Ebbesen, P. Ajayan, *Nature* **1992**, *358*, 220.
[17] J. Kong, H. T. Soh, A. M. Cassell, C. F. Quate, H. Dai, *Nature* **1998**, *395*, 878.
[18] T. Dürkop, S. Getty, E. Cobas, M. Fuhrer, *Nano Lett.* **2004**, *4*, 35.
[19] O. Kanoun, C. Müller, A. Benchirouf, A. Sanli, T. N. Dinh, A. Al-Hamry, L. Bu, C. Gerlach, A. Bouhamed, *Sensors* **2014**, *14*, 10042.
[20] Y. Zhu, F. Xu, *Adv. Mater.* **2012**, *24*, 1073.
[21] Y. Zhang, C. J. Sheehan, J. Zhai, G. Zou, H. Luo, J. Xiong, Y. Zhu, Q. Jia, *Adv. Mater.* **2010**, *22*, 3027.
[22] L. Cai, J. Li, P. Luan, H. Dong, D. Zhao, Q. Zhang, X. Zhang, M. Tu, Q. Zeng, W. Zhou, *Adv. Funct. Mater.* **2012**, *22*, 5238.
[23] K. H. Kim, Y. Oh, M. Islam, *Nat. Nanotechnol.* **2012**, *7*, 562.
[24] S. Wang, R. A. Dryfe, *J. Mater. Chem. A* **2013**, *1*, 5279.

[25] M. Chen, L. Zhang, S. Duan, S. Jing, H. Jiang, C. Li, *Adv. Funct. Mater.* **2014**, *24*, 7548.
[26] I. Y. Stein, B. L. Wardle, *Carbon* **2014**, *68*, 807.
[27] I. N. Kholmanov, C. W. Magnuson, R. Piner, J. Y. Kim, A. E. Aliev, C. Tan, T. Y. Kim, A. A. Zakhidov, G. Sberveglieri, R. H. Baughman, *Adv. Mater.* **2015**, *27*, 3053.
[28] Z. Yu, X. Niu, Z. Liu, Q. Pei, *Adv. Mater.* **2011**, *23*, 3989.
[29] C. Yan, J. Wang, W. Kang, M. Cui, X. Wang, C. Y. Foo, K. J. Chee, P. S. Lee, *Adv. Mater.* **2014**, *26*, 2022.
[30] J. J. Park, W. J. Hyun, S. C. Mun, Y. T. Park, O. O. Park, *ACS Appl. Mater. Interfaces* **2015**, *7*, 6317.
[31] E. Roh, B.-U. Hwang, D. Kim, B.-Y. Kim, N.-E. Lee, *ACS Nano* **2015**, *9*, 6252.
[32] E. Shi, H. Li, L. Yang, J. Hou, Y. Li, L. Li, A. Cao, Y. Fang, *Adv. Mater.* **2015**, *27*, 682.
[33] X. Li, W. Cai, J. An, S. Kim, J. Nah, D. Yang, R. Piner, A. Velamakanni, I. Jung, E. Tutuc, S. K. Banerjee, L. Colombo, R. S. Ruoff, *Science* **2009**, *324*, 1312.